Phys. Status Solidi RRL **7**, No. 12, 1041–1044 (2013) / **DOI** 10.1002/pssr.201308150

Rapid dislocation-density mapping of as-cut crystalline silicon wafers

David Berney Needleman[*, 1], **Hyunjoo Choi**[1, 2], **Douglas M. Powell**[1], **and Tonio Buonassisi**[**, 1]

[1] Department of Mechanical Engineering, Massachusetts Institute of Technology, 77 Massachusetts Avenue, Cambridge, MA 02139, USA
[2] Currently at: School of Advanced Materials Engineering, Kookmin University, 77 Jeongneung-ro, Seongbuk-gu, Seoul, 136-702, Republic of Korea

Received 31 August 2013, revised 16 September 2013, accepted 17 September 2013
Published online 2 October 2013

Keywords silicon, photovoltaics, dislocations, etch pits, optical microscopy

[*] Corresponding author: e-mail dbn@mit.edu
[**] e-mail buonassisi@mit.edu

Rapid quantification of structural defects, especially dislocations, is desired for characterization of semiconductor materials. Herein, we outline and validate a low-cost approach for dislocation-density quantification in silicon, involving a high-resolution commercial dark-field imaging device, a flatbed scanner. This method requires minimal surface preparation and can be performed on as-cut 15.6 × 15.6 cm^2 wafers in less than 5 minutes. The method has been tested at a spatial resolution down to 250 µm. At 1 mm resolution, the average root mean square of the normalized error was 0.39.

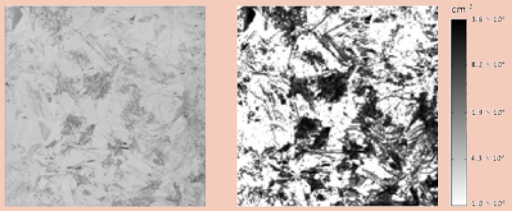

Flatbed scanner image of a defect-etched 15.6 × 15.6 cm^2 silicon wafer (left) and the corresponding dislocation-density map obtained using our technique (right).

1 Introduction Dislocations can severely reduce crystalline semiconductor device performance by introducing mid-gap defects that increase recombination [1]. In particular, dislocations limit crystalline silicon (c-Si) solar cell conversion efficiencies by limiting minority-carrier lifetime [2] and reducing the effectiveness of gettering [3]. Many commercial and pre-commercial c-Si materials suffer from the presence of dislocations, including cast multicrystalline silicon (mc-Si) [4], cast quasi-monocrystalline silicon [5], and various thin, kerfless silicon materials [6–8]. Characterizing the spatial distribution of dislocations across entire wafers is beneficial for achieving high performance with these materials, as localized areas of high dislocation density can dramatically reduce device performance [7, 8].

Mapping the density of dislocations is therefore of interest to the photovoltaic research community, even leading to the development of commercial mapping tools [9]. Yet, many dislocation-density measurements are conducted by: polishing the sample surface, using a chemical etch like Sopori [10] or Secco [11] to reveal dislocations, scanning the resulting etch-pits using a microscope connected to a camera, and using a software package to count the dislocation etch-pits. Since etch-pit sizes of 3–6 µm are typical, spatial resolution better than 1 µm is desired to resolve individual etch-pits. However, high-resolution microscope scanning is time-consuming in our laboratory. 1-µm-resolution microscope scans take ~1 hour per cm^2. Furthermore, this process requires mechanical or chemical-mechanical polishing, which can require intensive labor and expensive equipment. Commercial dislocation-counting systems greatly accelerate image acquisition, but are costly and still require optically flat surfaces to correctly count dislocations. Here, we present a rapid dislocation counting method that can map the dislocation density of 15.6 × 15.6 cm^2 wafers in less than 5 minutes using a flatbed scanner. Surface treatment before the dislocation-revealing etch is not necessary, although we found that an isotropic etch before the dislocation-revealing etch improves accuracy.

2 Methods We developed and tested this technique using standard wire-sawn mc-Si wafers. Our approach involved five steps:

(1) *Etching*. Dislocations were revealed by a 1-minute Sopori etch followed by cleaning with a 9:1::HNO_3:HF (9:1) dip. Measurements were also performed with a mild saw-damage etch (9:1) before the Sopori etch to reduce surface roughness. While reasonable results were obtained on unetched wafers, removing 10 or more μm of Si per side was found to improve the accuracy of the dislocation density measurement, with greater improvements with more material removed. Details can be found in the Results section below.

(2) *Scanning*. Wafers were scanned with an Epson Perfection V700 Photo Scanner at resolutions of 600 to 12,800 dots per inch (DPI). The scanner resolution was found to set a lower limit on the resolution of the dislocation density map. Details can again be found in the Results section.

(3) *Calibration.* Images were calibrated with a correlation to optical microscope counting of a representative region of the scanned wafer (Nikon Eclipse LV100 microscope, Q Imaging Retiga 2000R Fast 1394 camera, Dell T690 running NIS-elements software).

A single calibration was found to be valid for all wafers with similar surfaces scanned under the same conditions. Thus a small area of a single wafer could be used to calibrate a set of samples. To test the robustness of this technique, scanned images with resolution varied from 600 to 12,800 DPI and optical microscope images of the samples with a resolution of 32,000 DPI were obtained for a set of 1 cm^2 samples (both saw-damage-etched and as-cut). The scanner pixel counts were correlated to microscope dislocation counts for segments ranging in size from 1 to 11 mm^2. A linear relationship was found for all samples and test conditions.

(4) *Counting Algorithms.* Images were analyzed with MATLAB scripts developed at MIT [12] that are freely available online at http://pv.mit.edu/dlcounting/. Distinct, though similar, scripts were used to analyze scanner and microscope images. Starting from an image like the one on the left in Fig. 1a, both scripts first converted color images to grayscale, and thresholded them into pure black and white. Remaining image noise from surface texture and other artifacts were filtered out based on size (maximum and minimum dislocation sizes were specified by the user) and frequency (likewise user-specified), with size observed to be more important. The image was then inverted, so etch pit pixels could be counted (Fig. 1a, right). The image was then divided into segments of user-specified size. The segment size is the resolution of the final dislocation density map and must be chosen accordingly. However, larger segments gave more accurate dislocation density measurements.

At this point in the process, the scanner and microscope counting codes diverge. Within each segment, the microscope code divided regions of white in the segment into individual etch pits or clusters based on their size,

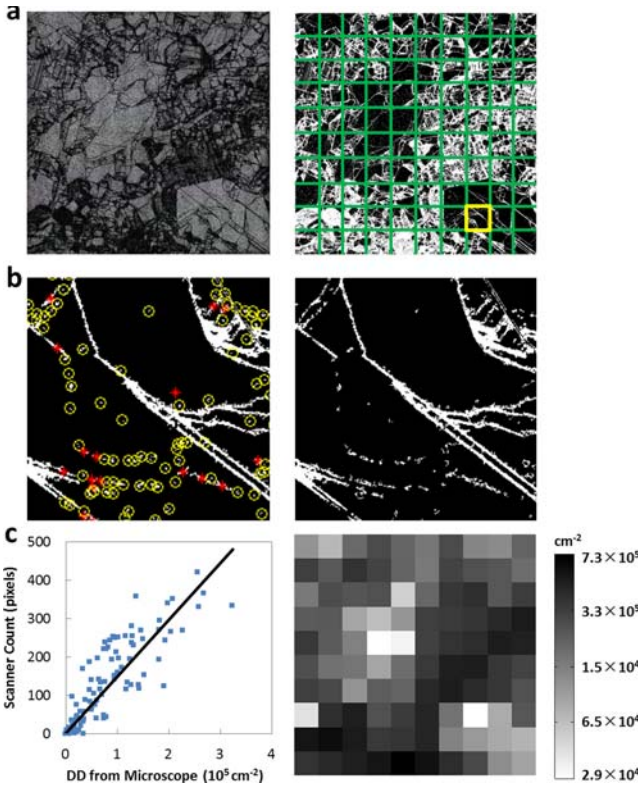

Figure 1 (a) Original image (left) of 1 cm wafer was thresholded, filtered, inverted, and divided into segments (right). (b) For individual segments (example highlighted in yellow), individual dislocations (yellow circles) and clusters (red stars) were counted for the microscope image (left) while the total number of white pixels was counted for the scanner image (right). (c) Each segment was used as a single point in the calibration plot (left), and a linear fit was obtained to relate the dislocation-density (DD) obtained from the microscope to the number of white pixels in a segment of a scanner image. This fitting was used to generate a DD map of the full scanned image (right).

again using the user-specified limits on individual etch pits. The number of individual etch pits were counted and their average size calculated. The number of etch pits in each cluster was determined by dividing the total cluster area by the average individual etch pit size (Fig. 1b, left). This method assumes dislocation etch pits do not overlap within clusters, limiting the dislocation density within clusters to less than ~4×10^6 cm^{-2} for 5 μm etch pits. The dislocation density was taken to be the total number of etch pits divided by the area of the segment in cm^2. The scanner script simply counted the number of white pixels within each segment (Fig. 1b, right).

Calibration curves were generated by measuring the same region with both the microscope and scanner counting methods. The number of white pixels from the scanner image was plotted against the dislocation density obtained from the microscope image for each segment, and a linear relationship was extracted by fitting these data (Fig. 1c, left).

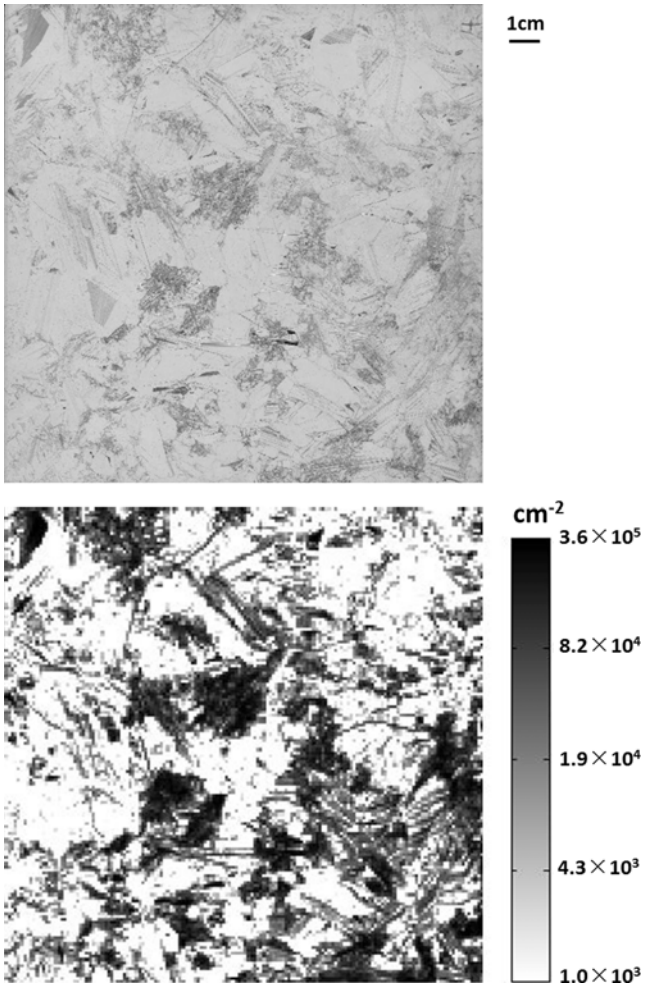

Figure 2 Scanned image (top) and resulting dislocation-density map (bottom), of $15.6 \times 15.6\ cm^2$ wafer after Sopori etching without a pre-etch surface treatment.

(5) *Mapping*. After calibration, dislocation density maps of full samples were generated from scanned images (Figs. 1c, 2). As noted earlier, each pixel in these maps corresponded to a single segment in the MATLAB algorithm. Furthermore, the mapping had to be performed with the same segment/pixel size as the calibration for the calibration fit to be accurate. The program algorithm was partially inspired by the work of Rinio and others [13–15].

3 Results and discussion Good correlation was found between dislocation densities obtained with the scanner and microscope for samples that were saw-damage-etched before Sopori etching as well as those that were not (Fig. 3). To quantify the error in the measurement, the difference between the dislocation-density measured by the scanner and the optical microscope was calculated for each segment and normalized by the microscope dislocation-density value for that segment. For the sample without a saw-damage etch, the average root mean square of this

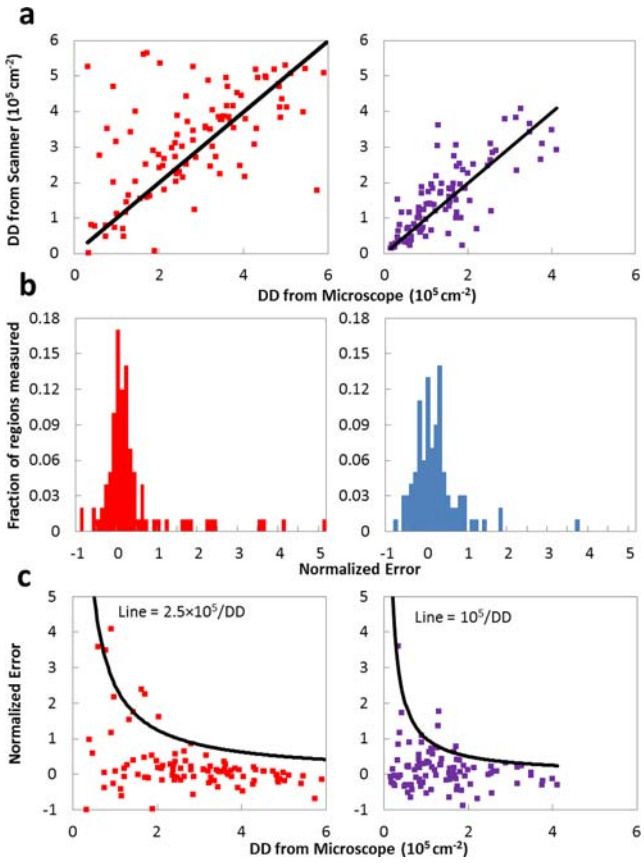

Figure 3 Comparison of DD measured by scanner and optical microscope for samples without (left) and with (right) a saw-damage etch prior to dislocation etching. (a) DD measured by scanner plotted vs. DD measured by microscope, with line indicating 1 : 1 correlation. (b) Histogram of the normalized error between flatbed scanner and optical microscope (ratio of the difference between the scanner DD value and microscope DD value to the microscope DD value in a given segment). (c) Ratio in (b) plotted vs. the microscope DD, with the line indicating the envelope function fit due to surface texture. A lower value implies better signal to noise.

error distribution was 0.62 (Fig. 3b, left). For the saw-damage-etched sample, the average root mean square of the error was 0.39 (Fig. 3b, right).

The improvement from the saw-damage etch appears to be due to a reduction in surface texture on the sample, which can result in dislocation "false positives." This surface texture seems to create a noise floor in the data indicated by the lines in Fig. 3c. The problem is likely compounded in areas of low dislocation density since these areas will contain more individual dislocations (as opposed to clusters), which appear more similar to surface texture in images. This similarity makes thresholding and filtering less effective at distinguishing between the two.

This method enables the counting of dislocations for a $15.6 \times 15.6\ cm^2$ wafer in less than 5 minutes. Furthermore, our approach significantly reduces the wafer polishing requirements for quantification of dislocation-density.

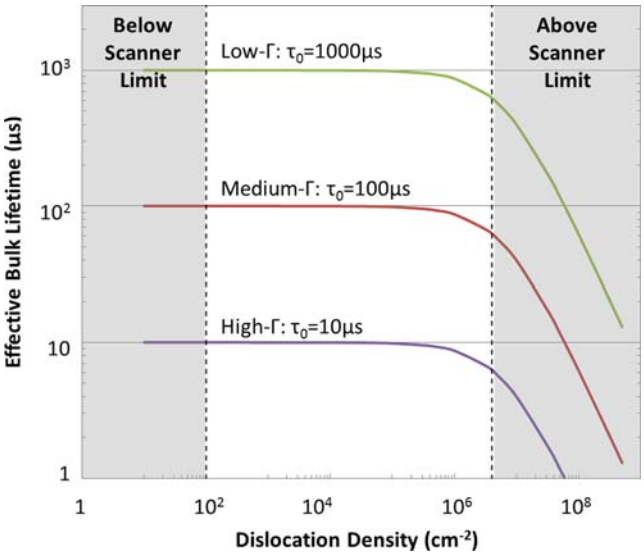

Figure 4 Upper and lower limits of dislocation density the scanner technique is able to measure, with lifetimes *vs.* dislocation density curves shown for different dislocation recombination strengths based on Refs. [2] and [16]. High-$\Gamma = 1.52 \times 10^{-2}$ cm^2/s, Medium-$\Gamma = 1.52 \times 10^{-3}$ cm^2/s, Low-$\Gamma = 1.52 \times 10^{-4}$ cm^2/s. τ_0 indicates the dislocation-free lifetime of the Si bulk.

However, we note several technical limitations of the technique. First, to be visible in scanned images (regardless of scanner resolution), etch pits must be at least 5 μm wide. As with the microscope counting algorithm, this sets a maximum measureable dislocation-density of approximately 4×10^6 cm^{-2}, as 5 μm wide etch pits overlap above this density. While a detailed study was not undertaken, experience has shown that even with polished samples, distinguishing dislocation-densities below 10^2 cm^{-2} is not feasible. Densities between 10^2 and 4×10^6 cm^{-2} are of interest in measurements, however, as these densities are sufficient to limit lifetime at a variety of recombination strengths in c-Si material with a wide range of contamination (Fig. 4).

As mentioned earlier, there is a trade-off between the size of the scanner image segments and the accuracy of the measurement. The data presented here is for a dislocation map with 1 mm^2 resolution, though resolutions down to 0.0625 mm^2 were tested successfully. Furthermore, the scanner resolution must be significantly higher than the image segmentation resolution to obtain reasonable results. For instance, 600 DPI was found to be sufficient for 0.25 mm^2 pixels but not for 0.0625 mm^2 pixels. Beyond setting a lower limit image segment size, scanner resolution was not found to have a significant effect on the accuracy of the measurement.

Acknowledgements We thank M. L. Vogl, S. Castellanos, C. Collin, and M. I. Bertoni for earlier development of the microscope counting method, J. Hofstetter for sharing data from early applications of the scanner DD technique, and B. L. Sopori for helpful conversations. This work was funded by the U.S. Department of Energy under DE-EE0005314. H. J. Choi acknowledges the support of the National Research Foundation of Korea funded by the Korean Government (NRF-2012-K1A3A1A30-054980). D. M. Powell acknowledges the support of the Department of Defense (DoD) through the National Defense Science & Engineering Graduate Fellowship (NDSEG) program.

References

[1] H. Alexander and H. Teichler, in: Electronic Structures and Properties of Semiconductors, edited by K. A. Jackson and W. Schröter, Handbook of Semiconductor Technology, Vol. 1 (John Wiley & Sons, Weinheim, 2000), chap. 6.
[2] C. Donolato, J. Appl. Phys. **84**, 2656–2664 (1998).
[3] B. L. Sopori, J. Electron. Mater. **31**, 972–980 (2002).
[4] C. W. Lan, W. C. Lan, T. F. Lee, A. Yu, Y. M. Yang, W. C. Hsu, B. Hsu, and A. Yang, J. Cryst. Growth **360**, 68–75 (2012).
[5] X. Gu, X. Yu, K. Guo, L. Chen, D. Wang, and D. Yang, Sol. Energy Mater. Sol. Cells **101**, 95–101 (2012).
[6] A. Augusto, D. Pera, H. J. Choi, P. Bellanger, M. C. Brito, J. Maia Alves, A. M. Vallêra, T. Buonassisi, and J. M. Serra, J. Appl. Phys. **113**, 083510 (2013).
[7] B. L. Sopori, V. Budhraja, P. Rupnowski, S. Johnston, N. Call, H. Moutinho, and M. Al-Jassim, in: Proc. 34th IEEE PVSC, Philadelphia, USA, 2009, pp. 1969–1974.
[8] K. Nakayashiki, V. Meemongkolkiat, and A. Rohatgi, IEEE Trans. Electron. Devices **52**, 2243–2249 (2005).
[9] B. L. Sopori, P. Rupnowski, V. Budhraja, M. Albert, C. Khattak, and M. Seacrist, MRS Proc. **1210**, Q01–02 (2009).
[10] B. L. Sopori, J. Electrochem. Soc. **131**, 667–672 (1984).
[11] F. Secco d'Aragona, J. Electrochem. Soc. **119**, 948–951 (1972).
[12] M. Vogl, Dislocation Density Reduction in Multicrystalline Silicon through Cyclic Annealing, S. M. Thesis, Massachusetts Institute of Technology, 2011.
[13] M. Rinio, Untersuchung der prozessabhängigen Ladungsträgerrekombination an Versetzungen in Siliziumsolarzellen, Ph.D. Thesis, Technische Universität Bergakademie Freiberg, 2004.
[14] V. Ganapati, S. Schoenfelder, S. Castellanos, S. Oener, R. Koepge, A. Sampson, M. A. Marcus, B. Lai, H. Morhenn, G. Hahn, J. Bagdahn, and T. Buonassisi, J. Appl. Phys. **108**, 063528 (2010).
[15] M. Bertoni, D. M. Powell, M. L. Vogl, S. Castellanos, A. Fecych, and T. Buonassisi, Phys. Status Solidi RRL **5**, 28–30 (2011).
[16] M. Rinio, S. Peters, M. Werner, A. Lawerenz, and H. J. Möller, Solid State Phenom. **82–84**, 701–706 (2002).

